Agència de Gestió d'Ajuts Universitaris i de Recerca

UNIÓ EUROPEA
Fons Social Europeu

Memòria justificativa de recerca de les beques predoctorals per a la formació de personal investigador (FI)

La memòria justificativa consta de les dues parts que venen a continuació:
1.- Dades bàsiques i resums
2.- Memòria del treball (informe científic)

Tots els camps són obligatoris

1.- Dades bàsiques i resums

Títol del projecte ha de sintetitzar la temàtica científica del vostre document.
Control of Optical Fields and Single Photon Emitters by Advanced Nanoantenna Structures

Dades de l'investigador (benficiari de l'ajut)

Nom: Lars
Cognoms: Neumann
Correu electrònic: lars.neumann@icfo.es

Dades del director del projecte

Nom: **Niek**
Cognoms: Van Hulst
Correu electrònic: **niek.vanhulst@icfo.es**

Dades de la universitat / centre al que s'està vinculat

ICFO-Institut de Ciències Fotòniques

Número d'expedient

2010FI-B200139

Paraules clau: cal que esmenteu cinc conceptes que defineixin el contingut de la vostra memòria.
Physics, Optics, Photonics

Data de presentació de la justificació

11/04/2011

Resum en la llengua del projecte (màxim 300 paraules)

Resum en anglès(màxim 300 paraules)
The control of optical fields on the nanometre scale is becoming an increasingly important tool in many fields, ranging from channelling light delivery in photovoltaics and light emitting diodes to increasing the sensitivity of chemical sensors to single molecule levels. The ability to design and manipulate light fields with specific frequency and space characteristics is explored in this project. We present an alternative realisation of Extraordinary Optical Transmission (EOT) that requires only a single aperture and a coupled waveguide. We show how this waveguide-resonant EOT improves the transmissivity of single apertures. An important technique in imaging is Near-Field Scanning Optical Microscopy (NSOM); we show how waveguide-resonant EOT and the novel probe design assist in improving the efficiency of NSOM probes by two orders of magnitude, and allow the imaging of single molecules with an optical resolution of as good as 50 nm. We show how optical antennas are fabricated into the apex of sharp tips and can be used in a near-field configuration

2.- Memòria del treball (informe científic sense limitació de paraules). Pot incloure altres fitxers de qualsevol mena, no més grans de 10 MB cadascun d'ells.

Control of Optical Fields and Single Photon Emitters by Advanced Nanoantenna Structures

Lars Neumann
Thesis Supervisor: Niek F. van Hulst
ICFO - The Institute of Photonic Sciences

21 February 2011

Abstract

The control of optical fields on the nanometre scale is becoming an increasingly important tool in many fields, ranging from channelling light delivery in photovoltaics and light emitting diodes to increasing the sensitivity of chemical sensors to single molecule levels. The ability to design and manipulate light fields with specific frequency and space characteristics is explored in this project. We present an alternative realisation of Extraordinary Optical Transmission (EOT) that requires only a single aperture and a coupled waveguide. We show how this waveguide-resonant EOT improves the transmissivity of single apertures. An important technique in imaging is Near-Field Scanning Optical Microscopy (NSOM); we show how waveguide-resonant EOT and the novel probe design assist in improving the efficiency of NSOM probes by two orders of magnitude, and allow the imaging of single molecules with an optical resolution of as good as 50 nm. We show how optical antennas are fabricated into the apex of sharp tips and can be used in a near-field configuration.

Keywords

Physics, Optics, Photonics

Contents

1 Waveguide-Resonance Extraordinary Optical Transmission

1.1 Introduction

Apertures smaller than the wavelength of the exciting light are an important tool in the manipulation of light fields. They allow the localisation of light fields into very small volumes and access to the optical near-field, properties, that are used in applications such as data storage or microscopy. Their transmissivity responds strongly to variations in the local dielectric function, making chemical sensing of biomolecules in low concentrations probably the most relevant application.

However, the transmissivity of such an aperture is fundamentally constraint by its sub-wavelength nature, and as the light field inside the aperture is evanescent in nature. Classical aperture theory by Bethe [1] predicts a steep fourth-power reduction in the transmission with the aperture diameter for any aperture in a thin metallic screen. A higher localisation of the light field can thus only be achieved at the cost of a strongly decreased transmission.

In 1998, T.W. Ebbessen et al. [2] showed how resonances can increase the transmissivity of an array of sub-wavelength apertures in thin, otherwise opaque metallic films. They named this phenomena "extraordinary optical transmission (EOT)" and showed that improvements in transmissivity of several orders of magnitude compared to classical aperture theory can be achieved. Furthermore, the transmissivity could even exceed unity when normalised to the area of the apertures in the film.

The excitation of plasmons at the surface of the periodically patterned metallic film and their constructive interference is responsible for the extraordinary optical transmission. The wavelength at which EOT happens thus depends critically on the exact sample parameters, such as the diameter of the apertures, the array lattice constant, and the material and thickness of the metallic film.

The transmission process can be seen as three consecutive, approximately decoupled processes: The coupling of a plane wave propagating in free space to a plasmon confined to the surface of the film; the coupling through the aperture; and the out-coupling on the other side of the film of a surface plasmon to a wave propagating in free space again. Viewing EOT as a sum of several independent, however in some parameter matched processes paths the way to realise EOT also in other systems.

Here, we propose and implement an alternative realisation of EOT that does not require an array of apertures or a grating structure; instead it uses resonant coupling to a waveguide [3].

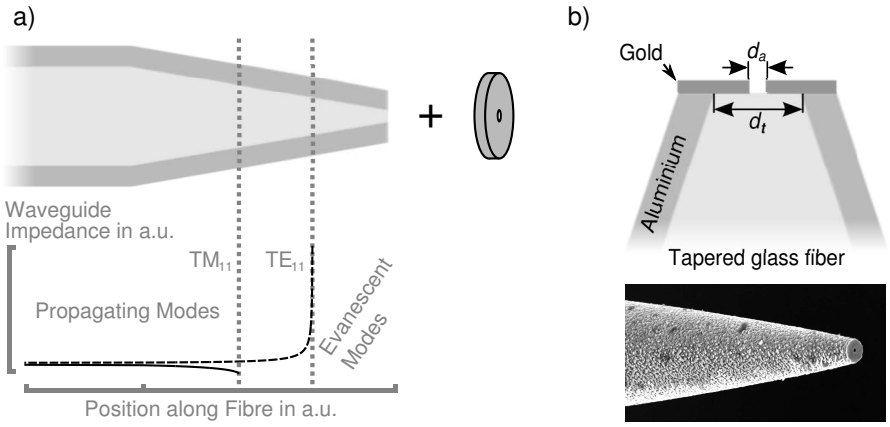

Figure 1: (a) The impedance of a mode diverges near its mode cut-off. Placing a single aperture with a fixed impedance at a specific position in a tapered waveguide allows to match the impedance of the waveguide with the impedance of a single aperture. (b) The proposed design (above) and its realisation (below).

Figure 1a shows how the impedance of an aperture and a waveguide can be matched to yield what we name "waveguide-resonant extraordinary optical transmission (WR-EOT)" in the following. The waveguide is tapered such that the propagating modes within the waveguide experience a cut-off point corresponding to a certain taper diameter beyond which they cannot propagate anymore. This cut-off diameter is different for every mode, and is always larger than the diffraction limit.

The WR-EOT occurs for wavelengths above the cutoff of one of the higher-order TM modes in the waveguide. Approaching the cutoff, the admittance of that waveguide mode diverges, as does the admittance of the aperture as it is made infinitesimally small. Therefore, the transmission phenomenon may be considered as a problem of impedance matching, where the energy builds up resonantly in the TM mode above its cutoff. This phenomenon is similar to EOT in aperture-arrays, where surface waves store the energy to allow for enhanced transmission at wavelengths longer than the Wood's anomaly; except here, only a single aperture is present. A criterion for WR-EOT is that the mode inside the fiber has a divergent transverse magnetic field at its cutoff wavelength, which enhances the coupling to the aperture through Bethes theory [1]. Various TM modes may be chosen to satisfy these criteria; however, the TM_{11} mode was selected in this case because it is the lowest order mode that allows for a concentric apertures (i.e., it has a non-zero transverse magnetic field in the center of the waveguide). This cutoff mode inside the fiber is evanescent away from the metal film at the NSOM tip, therefore, it is equivalent to a surface wave, and its energy is stored near the surface with the aperture. This is analogous to the surface waves in EOT of hole arrays, except that here the geometry of the fiber replaces the periodicity of the array. The mode cutoff, which is analogous to the Wood's anomaly wavelength in the array case, is given by [4]:

$$\lambda_C = \frac{\pi d_t n_f}{3.832} \tag{1}$$

where is the refractive index of the fiber, is the final taper diameter and it is assumed for simplicity that the aluminum coating is a perfect electric conductor. Fig. 3 shows the location of the cutoff predicted by this equation as a red line. Indeed Eqn. 1 describes the trend, yet it is clear that the peak resonant transmission occurs for wavelengths slightly longer than the cutoff of the TM_{11} mode.

1.2 Sample Fabrication

As pointed out in the previous section, the wavelength at which WR-EOT occurs is determined by the diameter of the taper at which the aperture is placed. Keeping the parameters of the aperture, and with

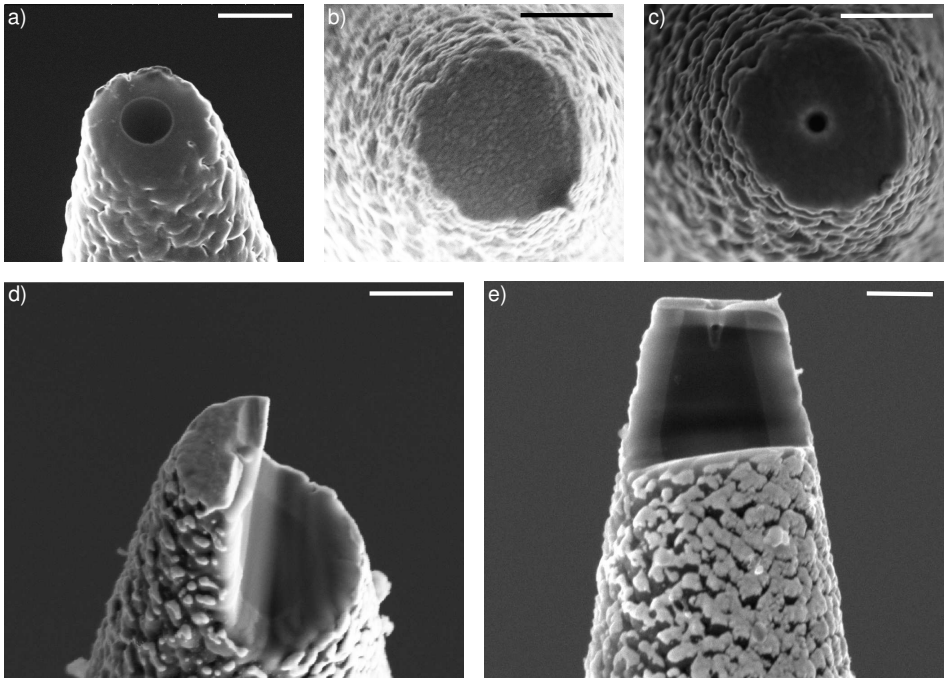

Figure 2: (a-c) The three steps of the fabrication process. (a) The tapered fibre waveguide is cut at the final taper diameter and the tapered glass core coated with a thick Aluminium layer in order to prevent light leakage. (b) A Gold layer of 100 nm in thickness is deposited on the facet. (c) A focused ion beam cuts the aperture into the Gold layer. Its diameter is held constant at 100 nm. (d-e) Cross sections show the inside of the fabricated probes. The very different sputtering rates of the soft Gold and the harder Glass and Aluminium faces introduce imaging artefacts around the aperture.

that its impedance, constant will then yield in a relation between taper diameter and WR-EOT wavelength that can be measured and compared to theory.

Therefore, the parameter varied in the fabrication is the final taper diameter at which we place the aperture. As the measurements are carried out at wavelengths of visible light, we choose an optical fibre as the waveguide.

The design presented in Figure 1b is realised in a three step process. First, the taper is fabricated by heat-pulling an optical fibre. A thick coating of 220 nm of Aluminium prevents unwanted light leakage from the taper region that would otherwise add a strong background to the aperture signal in the optical mesurements. We use a focussed ion beam to cut the taper to the desired final taper diameter. Figure 2a shows the probe in this stage. In the second step the facet of the probe is coated with a Gold layer of 100 nm in thickness (2b).

The final step consists in milling the aperture into the Gold layer on the facet, for which again focused ion beam equipment is used (Figure 2c). The diameter of the aperture is held constant at 100 nm, and careful alignment of the beam intensity ensures that aperture is milled only through the Gold layer and not into the Glass core of the fibre waveguide.

Figures 2d and e show cross sections of the final probe. Due to the different sputtering rates of Gold, Glass and Aluminium, the softer Gold layer on the facet with the aperture has been removed further than the waveguide.

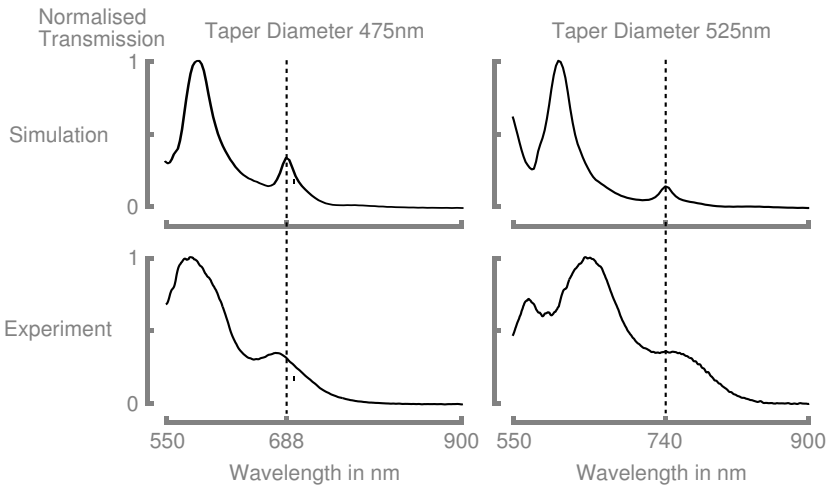

Figure 3: Simulations (top row) and experimentally recorded transmission spectra (bottom row), are shown exemplary for two fiber probes with final taper diameters of 475 nm (left column) and 525 nm (right column). The dashed lines indicate the transmission peak where the TM_{11} mode at cutoff in the tapered fiber waveguide couples resonantly to the aperture and extraordinary transmission is observed.

1.3 Set-up and Experiment

The quantity of interest is the wavelength at which impedance matching between the waveguide and the aperture occurs, and the transmission becomes enhanced over the non-resonant case.

We determine this wavelength by recording the out-coupling transmission and in-coupling collection spectra with a supercontinuum and a thermal light source. For the transmission spectra, the supercontinuum source is coupled to a commercial single mode fibre which is coupled to the sample fibre waveguide by a fibre-fibre connector. The end of the fibre waveguide with the aperture is then mounted on an xyz stage and positioned in the entrance slit of the spectrometer. For the in-coupling collection spectra, the aperture is placed in front of a white light source and the other end introduced into the fibre port of the spectrometer.

1.4 Results

Figure 3 shows experimental and numerically simulated spectra of two fibre probes with different final taper diameters. The good agreement between experimental data and the performed simulations is clearly visible. As WR-EOT is related to the cut-off of the TM_{11} mode, we attribute the peak at the longest wavelength for each fibre to WR-EOT.

In Figure 4 we have plotted the wavelengths of these peaks for several fibre waveguide probes against their final taper diameter and compare the experimental values to numerical simulations and a simple analytical model.

The expected linear dependence of the taper diameter is clearly confirmed by the experiments, and the simulations accuratly predict the wavelengths of the transmission peaks. The simple analytical model does not take into account the penetration depth of the light into the metal at optical wavelengths. Hence it underestimates the effective final taper diameter by the penetration depth and is shifted to shorter peak wavelengths.

The experimental results clearly prove the existance of waveguide-resonant extraordinary optical transmission [5].

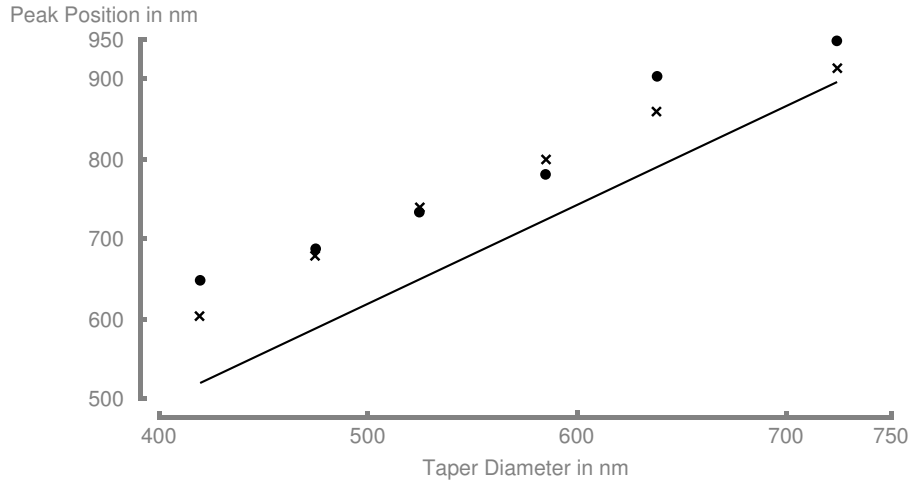

Figure 4: The spectral positions of the transmission peaks attributed to mode cutoff. The numerical simulations (crosses) are in good agreement with the experimental data (circles) and confirm the existence of the waveguide resonant extraordinary optical transmission. Indicated by the red line is the cutoff wavelength corresponding to the TM_{11} mode as predicted by Eq. 1 for a perfect electric conductor.

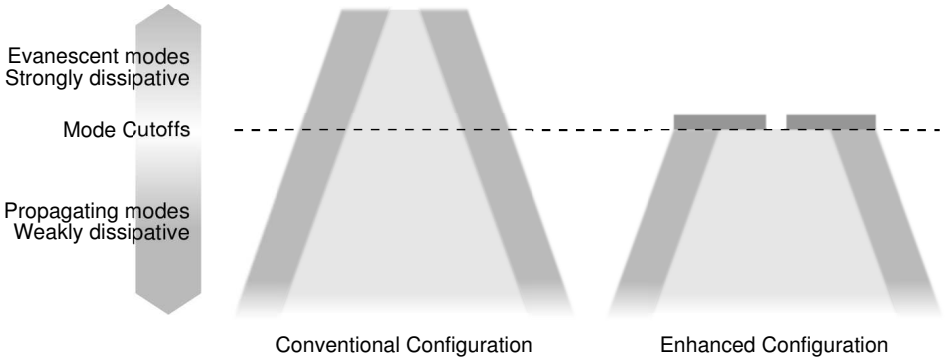

Figure 5: Compared to the conventional configuration of NSOM probes, the enhanced configuration lacks a sub-wavelength taper where all modes become evanescent in nature.

2 High Throughput Fibre Probes for Near-Field Optical Scanning Microscopy

2.1 Introduction

Near-field scanning optical microscopy (NSOM) combines optical microscopy with scanning probe microscopy to achieve an optical resolution well beyond the diffraction limit. Technically, an NSOM probe is usually realised by a single, subwavelength aperture that is formed by tapering an optical fibre and coating its side walls to prevent light leakage. However, the very low throughput of conventional NSOM fibre probes of typically only 10^{-5} to 10^{-7} [6] strongly constrains the widespread applicability of this technique.

Here we show how the probe design proposed in the previous section offers a convenient way to a higher throughput and a higher damage-threshold of near-field fibre probes.

Figure 5 shows why throughput and damage threshold are strongly constrained in fibre probes. Beyond the cut-off, a mode cannot propagate anymore along the fibre. Its energy either is transfered to other, lower order modes, becomes reflected, or dissipates into heat. Also, at cut-off this mode becomes evanescent in nature. The fraction of this exponentially decaying field that reaches the aperture depends on how far from the aperture the cut-off happens; it thus depends on the mode volume.

Thus, a large fraction of the launch power in each mode is dissipated into heat at and beyond its cut-off. The proposed design, however, lacks a sub-wavelength sized taper. Dissipation is strongly suppressed, which should increase the damage threshold. As the light field is evanescent only within the aperture but not the fibre, the field exiting the aperture had less decay length to cover. This is expected to increase the throughput of the enhanced design.

As we show, a higher throughput and damage threshold allow to decrease the aperture size and thus increase the resolution, which, for conventional NSOM probes, is limited to around 100 nm for practical reasons.

2.2 Sample Fabrication

The fabrication is identical to that in section 1.2. However, instead of keeping the aperture parameters invariant, we fabricate probes with small apertures as small as 50 nm.

2.3 Set-up and Experiment

We determine the throughput of the enhanced NSOM fibres and their damage threshold by placing the end of the fibre probe with the aperture in front of a large photo detector and couple laser light into the fibre. In case of the damage threshold, we record the input and transmitted power and than increase the input power until the aperture is destroyed. In case of the throughput, this measurement is carried out once at a power sufficiently lower than the expected damage threshold. For the sake of comparision, the throughput of several fibre probe were measured in the conventional configuration; they were then processed to the enhanced configuration and their throughput recorded again.

Finally, we measure the performance of the enhanced probe configuration in a home-built NSOM set-up on single fluorescent molecules. TDI molecules dissolved in Toluene/PMMA solution were spin coated on a glass slide and excited through the near-field of the fiber probe at a wavelength of 647 nm. The fiber probe was scanned over the sample with nanometric accuracy and the fluorescence signal of single molecules recorded with an avalanche photodetector.

2.4 Results

In Figure 6 we compare the transmissivity of conventional and enhanced probes. Some of the probes were fabricated in both configurations; this rules out any impact of variations in the taper shape on the transmissivity.

NSOM probes in the enhanced configuration show a clear improvement of two orders of magnitude in transmissivity over conventional probes for comparable aperture sizes. This is also confirmed by the numerical simulations presented in the figure which were fitted to the experimental data to account for any losses not included in the simulations.

To be stressed here is the fact that the optical transmission for a 50 nm aperture in the enhanced configuration is still significantly larger than for a 100 nm aperture in a conventional NSOM probe. Thus, the two orders of magnitude improvement in transmission are equivalent to a reduction in aperture diameter by over a factor two.

As mentioned before, we also expect an increased damage threshold in the enhanced configuration. And in fact, the enhanced configuration yields an improvement by approximately a factor 40. We explain this improved damage threshold by a combination of reduced absorption due to an enhanced coupling efficiency and lower optical intensities due to the broader probe design and the cutoff of the lowest order mode, effectively reducing the heat load on the metal coating.

Figure 7 shows fluorescence measurements of single TDI molecules. The fluorescence spot shows a confinement to 61 $\pm$ 3 nm (FWHM), which is close to the aperture diameter of 45$\pm$10 nm, as determined from SEM images of this specific fibre. The slightly larger size of the fluorescence spot is attributed to the

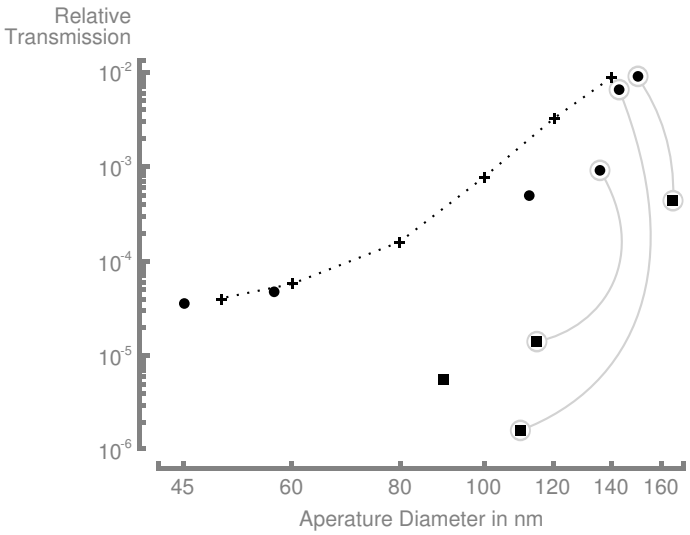

Figure 6: The figure shows the relative transmission as a function of the aperture diameter at a wavelength of 647 nm. The transmission in the enhanced configuration (circles) is two orders of magnitude larger than for conventional NSOM probes (squares) for comparable aperture sizes and agrees well with our numerical simulations (crosses, line is guide for the eye). The simulated throughput is fitted to the experimental data in order to account for losses not included in the simulations. Some of the fibre probres were first fabricated as conventional NSOM probes and then porcessed into the enhanced configuration; data points belonging to the same probe are connnected by gray lines.

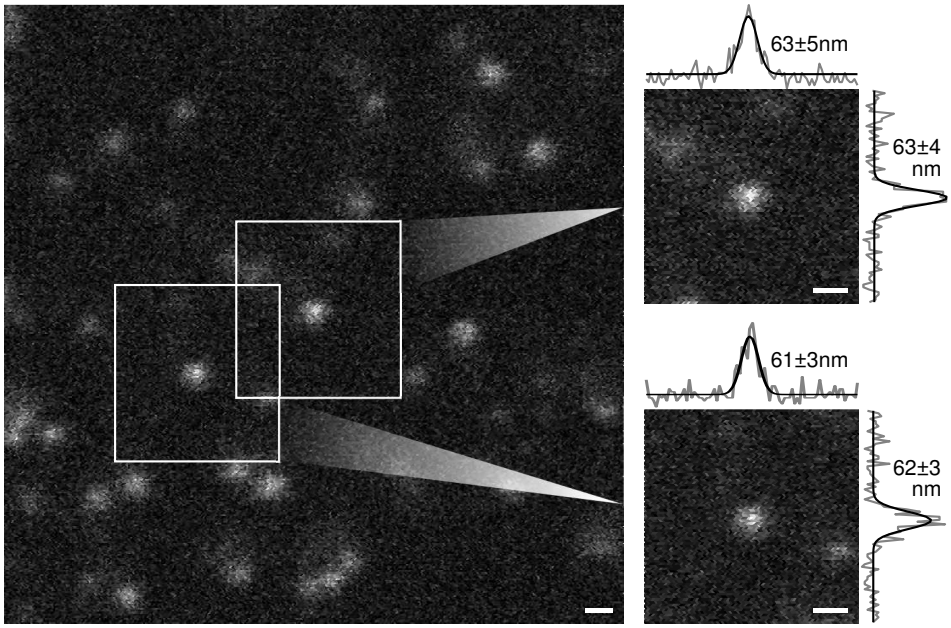

Figure 7: A scan across single TDI molecules with an enhanced NSOM probe with an aperture diameter of 45 nm reveals the improved resolution. The molecules were embedded in a PMMA matrix and excited at a wavelength of 647 nm. The spatial width of the fluorescence spot is 61 $\pm$ 3 and 62 $\pm$ 3 nm, respectively. The scale bar is 500 nm.

penetration of the electric field into the gold film, which increases the effective aperture size, and to the finite aperture-molecule distance.

In conclusion, we have shown the applicability of the proposed, enhance probe design for near-field applications. Furthermore, we have proven that an increase in resolution by a factor two can easily be achieve with this design [5].

3 Optical Antennas

3.1 Introduction

In the past years, optical antennas have gained increasing attention for their ability to confine propagating radition into a localised, not diffraction-limited volumn [7]. Important applications include photovoltaic and and chemical sensing where the control and manipulation of localised light fields promises to improve efficiency and sensitivity.

Many key properties of optical antennas are different from antennas designed for the radiowave regime; on the physical side, metals do not act as perfect conductors at optical frequencies anymore, introducing retardation effects and requiring corrections in the antenna designs. On the technical side, optical antennas extend only a few 100 nm at most. Even for state-of-the-art facilities, routinely fabricating structures of these dimensions remains a challenge, and large-scale applications still remain to be realised.

Experimentally investigation of optical antennas is challenging due to their small size. Features of interest occur on length scales similar to the diffraction limit, and there are only a few techniques that allow to investigate properties as the local field and the nature of an antennas interactions with its environment.

The most complete set of information can be drawn from placing a single emitter close to an optical antenna. The challenge here lies in the positioning of the single emitter (antenna) with respect to the antenna (single emitter) which requires nanometric control.

We can reach this nanometric control by fabricating the antenna into the facet of a sharp tip which is then scanned across single molecules. Our set-up allows to scan both the single emitter and the antenna on the sharp tip independently of each other, giving us access to the full mode profile of the antenna, and the interaction between both.

3.2 Sample Fabrication and Experiment

The set-up we performed the experiments with is an NSOM set-up; similar to an AFM, a tip is brought in nanometric contact to a sample surface. A confocal optical system allows to record the fluorescence signal with single-molecule-sensitivity.

We fabricate the tip from heat-pulling an optical fibre; while in aperture NSOM the fibre is also used to guide light, we operate in aperture-less NSOM and use the optical fibre only as a mean to fabricate a sharp glass tip. In a second step, we mill a flat plattform with a diameter of 500 nm or larger at the apex of the tip. A Gold layer on the flat apex forms the base for the optical antenna which we mill with a focused ion beam into the layer.

Figures 8 and 9 show some of the calibrations for the fabrication of optical antennas. For the milling process we used an approach based on lithography software; the designs were generated beforehand, and the impact of important parameters as the design dimensions and the milling doses and direction could be determined on test samples. As test samples we took flat glass substrates which were coated with identical layers as the sharp tips. This ensures high reproducibility when confering the results of the calibration upon optical antennas on sharp tips.

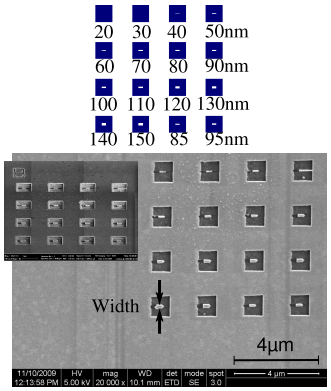

Figure 8: Careful calibration of the fabrication process helped in increasing quality and reproducibility. Here we investigate the impact of different widths in the lithography design on the actual milled antenna on a test sample. The upper part shows the lithography design, and the lower part shows a top and side view of the milled array.

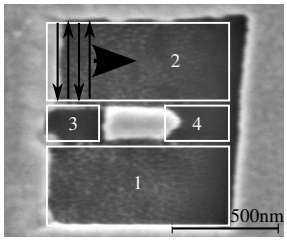

Figure 9: The milling direction, either towards, along or against the antenna, impacts the exact shape via redeposition processes, here visible on the right of the antenna structure.

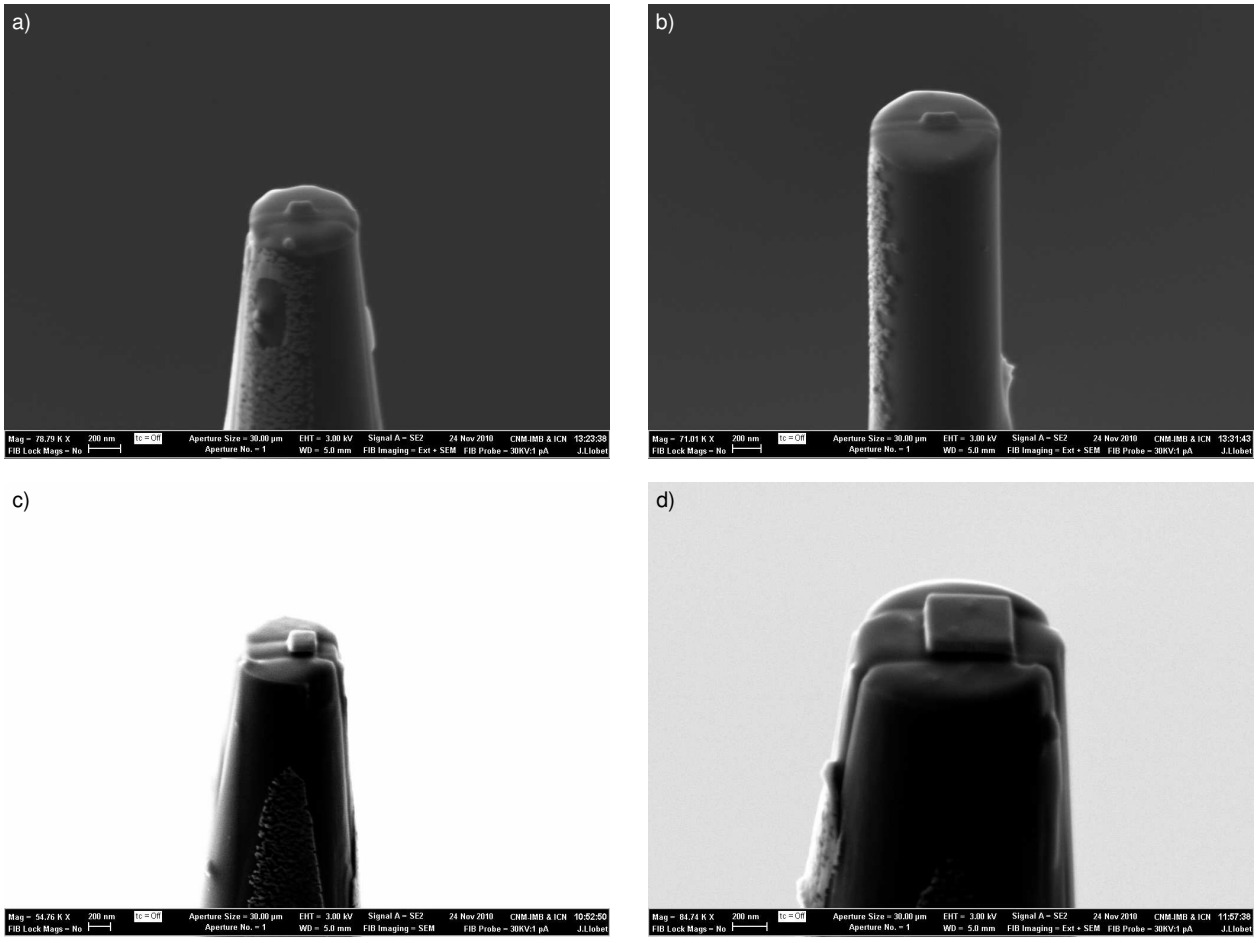

Figure 10: Examples for optical antennas fabricated into the facets of optical fibres. The antennas are milled from a 90 nm Gold layer deposited on the flat facet. (a)-(b): Monomer antennas with different lengths (130 nm × 40 nm × 30 nm and 210 nm × 40 nm × 30 nm). (c)-(d) Patches of different sizes (200 nm × 200 nm × 50 nm and 410 nm × 410 nm × 50 nm).

3.3 Results

Figure 10 shows some of the fabricated optical antennas. As the resonant properties are dependent on the exact dimensions of the optical antenna, we fabricated structures with different sizes. Figure 10a und b show monomer antennas which consist of only a single bar. The antenna in 10a has dimensions of 130 nm × 40 nm × 30 nm, while the length of the antenna in 10b has been extended to 210 nm. Figures 10c and d show Gold patches of 200 nm × 200 nm × 50 nm and 410 nm × 410 nm × 50 nm, respectively. The images show very well the level of control with which we are able to address the desired dimensions of optical antennas.

References

[1] H.A. Bethe. Theory of diffraction by small holes. *The Physical Review*, 66:163, 1944.

[2] T.W. Ebbesen, H.J. Lezec, H.F. Ghaemi, T. Thio, and P.A. Wolff. Extraordinary optical transmission through sub-wavelength hole arrays. *Nature*, 391:667, 1998.

[3] R. Gordon. Bethes aperture theory for arrays. *Physical Review A*, 76:053806, 2007.

[4] D.M. Pozar. *Microwave Engineering*. Wiley, 2004.

[5] L. Neumann, Y. Pang, A. Houyou, M.L. Juan, R. Gordon, and N.F. van Hulst. Extraordinary optical transmission brightens near-field fiber probe. *Nano Letters*, 11:355, 2011.

[6] G.A. Valaskovic, M. Holton, and G.H. Morrison. Parameter control, characterization, and optimization in the fabrication of optical fiber near-field probes. *Applied Optics*, 34:1215, 1995.

[7] N. van Hulst and L. Novotny. Antennas for light. *Nature Photonics*, 5:83, 2011.

List of Figures